The concept of reference curves for constitutive modelling in soil mechanics

Dorival M. Pedroso *, Daichao Sheng, Jidong Zhao

Centre for Geotechnical and Materials Modelling, The University of Newcastle, University Drive, Callaghan, NSW 2308, Australia

Abstract

This paper presents a simple concept which can be used for simulating a range of soil mechanics problems. The study is motivated by the observation that many experimental results are commonly described in terms of lines or curves according to a phenomenological approach. Frequently, these relations are based on rather different formulations from one application to another, and in complex forms for some cases. This leads to complications for the calibration of parameters as well as constitutive modelling. Thus, a general framework referred to as "reference curves" has been developed. This framework provides a unique treatment of the macroscopically observed behaviour of clays, sands, and structured materials under isotropic compression, as well as the water retention characteristics of granular materials and geotextiles. Several examples are provided illustrating the good accuracy of models developed with this concept. The proposed framework may be equally applied to any other behaviour where reference lines are easily identifiable from a macroscopic scope, such as some non-linear failure envelopes for granular materials. In addition, we show that the incorporation of the proposed equations into constitutive models is quite straightforward.
© 2008 Elsevier Ltd. All rights reserved.

Keywords: Constitutive models; Reference curves concept; Clays; Sands; Structured materials; Geotextile; Isotropic compression; Water retention

1. Introduction

The theory of soil mechanics has long been based on experimental investigations, where a common practice in determining various relations for soils is through observations and curve-fitting techniques seeking to provide linear or non-linear approximations for some predefined state variables. A well known example is the Cam clay theory, where the bilinear relations between the void ratio and the logarithm of mean effective stress for the isotropic normal compression line (NCL) and for the unloading–reloading line (URL) were adopted [14]. Linear relations, though having obvious advantages of simplicity and ease to calibrate and implement, are difficult to find in many occasions.

The relation between the void ratio of most sands and the applied compression pressure, for example, generally yields a curve rather than a line as in clays. Indeed, this non-linear compression relation for sands holds regardless whether it is plotted in a semi-log plane or in a double-log plane (e.g. [6,11,18,17]). Other examples of non-linear relations in soil mechanics include the isotropic compression of some naturally deposited soils that exhibit inherent initial structure [5,8], and the water retention characteristics of unsaturated media [3,16,15].

In order to consider non-linear relations in constitutive modelling of soils, various forms of mathematical formulae have been proposed, which, in many cases, are either too simple to fully describe the material behaviour, or too complex with many parameters without clear physical meanings. More importantly, these formulations are always problem-specific and thus only useful for some particular behaviour while mostly inapplicable to others. A general, flexible yet convenient framework is therefore much sought.

---

* Corresponding author. Tel.: +61 2 4921 5735; fax: +61 2 4921 6991.
E-mail address: dorival.pedroso@gmail.com (D.M. Pedroso).

In this paper, considering a phenomenological approach, where no explicit reference to microscale properties such as porosity, grain size, or density are made, we propose to employ reference lines as foundation for the prediction of some studied behaviour. Overall combined effects of the microstructure are modelled by casting the macroscale theory in terms of macroscale variables that are realistic to measure in the laboratory. In this manner, the slopes of the references lines are determined directly from results from mechanical or hydraulic tests, observed by means of relations between predefined state variables and plotted as experimental curves. Analytical formulations for simple cases are developed and incremental relations for more complex situations are provided. Both set of equations can be easily incorporated into constitutive models and, thus, be used with boundary problems solvers such as the finite element method.

Three set of equations are developed following the "reference curves" concept: the first one applies to situations where two reference lines can be easily identified; the second set of formulae can be used for the case where three references can be observed in which one reference line is near horizontal; and the last one is similar to the previous case; however, one of the reference lines is near vertical. The equations proposed are then applied to the simulation of the behaviour of isotropic compression of sands and structured materials and to the water retention characteristics of unsaturated soils and geotextiles, where the determination of all parameters is explained. In all these cases, the predictions agree very well with the experimental data. Therefore, we conclude that this technique is quite versatile and accurate. In addition, we believe that the simulation of the non-linear failure envelopes of some granular materials can also be predicted using this technique, as will be shown in a future study.

In the remainder of this paper, we will give an overview of some common observed behaviour in soil mechanics, deduce the equations of the three cases based on the "reference curves" concept mentioned above, compare model predictions with experimental data, and, in the appendixes, present all computer code necessary for the computation of predicted results after some conclusions are made.

2. Some common observations of different problems of soil mechanics

2.1. Isotropic compression of sands

A typical isotropic compression curve for sands exhibits three characteristic stages, AB, BC and CD as in Fig. 1. Each stage is associated with a particular deformation mechanism. The first stage (AB) is typically characterised by particle rearrangements in the form of sliding and rotation, whilst during the second stage (BC) particle crushing and further rearrangements occur when the applied pressures are high. The last stage (CD) represents a residual state where particle crushing is no longer the main
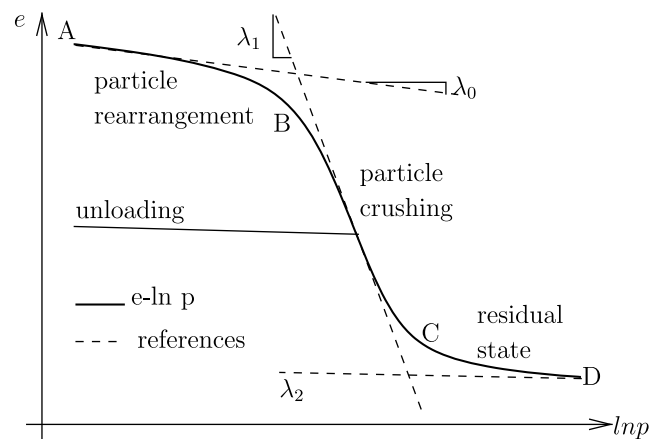

Fig. 1. General isotropic behaviour of sands.

deformation mechanism. Regarding the plane with coordinates being the void ratio and logarithmic mean effective stress (e–$\ln p'$), it is convenient to define three parameters, λ_0, λ_1, and λ_2 in order to represent the main inclinations observed at each stage. Note that these three inclinations can be directly determined from experimental data and also are related to a certain physical behaviour.

The transition from one state to another is somehow regulated by the energy of deformation involved. This energy may be measured by the area below the volumetric strain–mean stress curve. A parameter related to this relation may be defined. Thus, the area below the A–B–C section, related to the rearrangement-crushing transition, is defined by a parameter, symbolised by $\overline{\overline{\beta}}$. For the transition B–C–D, if the curvature is very different than that for the A–B–C section, an additional parameter, related to the residual phase transition and symbolised by $\overline{\beta}$, can be introduced.

The notation with two bars over the beta symbol is due to the way the formulae are deduced, as shown later, in which the equations using $\overline{\overline{\beta}}$ are obtained after the equations with $\overline{\beta}$. Thus, the equations for the "final" portion of the predicted curve, for higher values of abscissa (e.g. mean stress or suction), are deduced firstly, considering $\overline{\beta}$.

2.2. Water retention characteristics

Fig. 2 shows typical water retention curves for unsaturated soils and geotextiles. The drying curve can be characterised by three reference lines. At lower values of suction, the tangent to the drying curve has an inclination close to λ_0, while at higher suction levels a tangent line to the residual part with inclination of λ_2 can be observed. Note that in some existing models, both λ_0 and λ_2 have been assumed equal to zero for simplicity. For intermediate level of suction, a main inclination indicated by λ_1 can be observed.

The curvature for drying and wetting paths can be different; however, for simplicity, they will be considered to be equal. In fact, here, the hysteresis is not accounted for explicitly, but may be considered by incorporating a shift
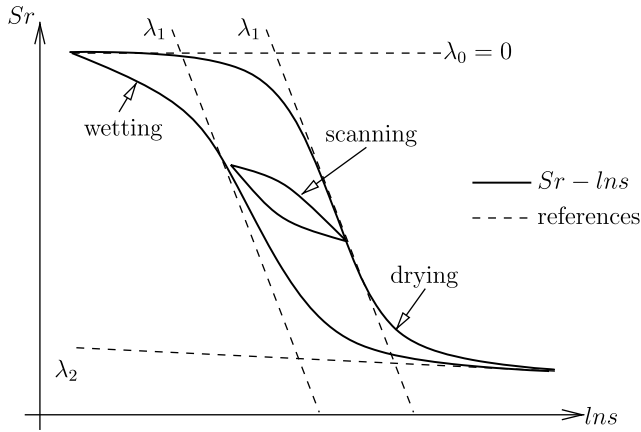
Fig. 2. General water retention characteristics.

from the drying curve to the wetting curve. In addition, the curvature of these curves close to $Sr = 1$ are considered different than the curvature close to the end part when $Sr \sim 0$. Therefore, a $\overline{\beta}$ parameter is adopted for the initial portion of the drying curve and $\overline{\overline{\beta}}$ for the final portion.

2.3. Volumetric behaviour of structured materials

Natural clays or structured materials can exhibit a different stress–strain relationship than the behaviour of the same material after loss of structure, for example, after remoulding. The difference is characterized by a stiffer volumetric response under isotropic compression, as can be observed by the non-linear stress–strain curve in the e–$\ln p'$ plot shown in Fig. 3. The "structured curve" can approach the normal consolidation line (NCL) after destructration, at higher values of mean effective pressure. For over-consolidated structured clays, an initial region of elastic behaviour may be observed as well, before the void ratio–mean stress state values reach the NCL. Therefore, three references may be conveniently identified: (a) an initial line with inclination close to λ_0, corresponding to the elastic compression; (b) a curve with main inclination equal to
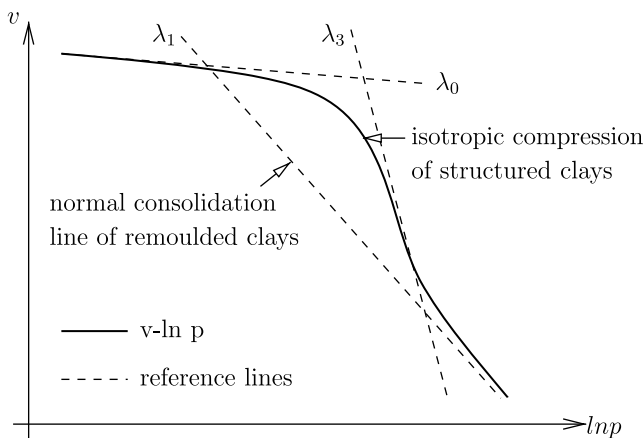

Fig. 3. General volumetric behaviour of structured materials.

λ_3, corresponding to the structured behaviour; and (c) the NCL with inclination equal to λ_1.

Likewise, the transitions on each section of the "structured curve" can be simulated by means of two constitutive parameters $\overline{\beta}$ and $\overline{\overline{\beta}}$. The first one, $\overline{\beta}$, will be considered for the elastic-structured transition and the second one, $\overline{\overline{\beta}}$, for the structured-normal consolidation transition at the section with higher values of mean stress on the non-linear compression curve.

3. Formulation

The equations for the simulation of the three examples mentioned in the previous section can be cast into a unique framework considering the common geometric (macroscopic) observations. The idea is to obtain an incremental relationship for the main pre-defined state variables. This relationship will be represented by a curve controlled by some additional reference lines by means of the "distances" from the current state to key points on the reference lines. These key points are viewed as internal variables. The incremental equations can then be directly incorporated in a constitutive model. An analytical expression is deduced for the simple case where only two references are identified.

The formulation is presented in a generic form using x and y as state variables. For example, the isotropic compression can be simulated by substituting x with $\ln p'$ and y with e, $\ln e$, or $\ln v$, where p' is the mean effective stress, e the void ratio, and $v = 1 + e$ the specific volume. For the water retention curve, we can substitute x with $\ln s$ and y with Sr or θ_w, where $s = u_a - u_w$ is the matric suction, u_a the air pore-pressure, u_w the water pore-pressure, Sr the degree of saturation, and θ_w the water content. Note that any other combination of state variables is possible as well.

The internal variables (key points) are tagged with "R" in order to indicate their nature as points on "reference" curves. For example, x_R or y_R indicate x reference value and y reference value, respectively. Three groups of equations are deduced: (a) considering two references lines; (b) considering three references – case 1, in which a horizontal distance and a vertical distance are considered; and (c) considering three references – case 2, where two horizontal distances are considered. The first one (a) can be applied to the isotropic compression of sands; the second (b), to the water retention behaviour; and the last (c) to the structured volumetric behaviour. We will start with a simple case of two reference lines, for which an analytical solution is provided.

3.1. Two references

The case when only two reference lines can be identified is illustrated in Fig. 4. In this figure, the curve denoted by $y(x)$ represents some non-linear behaviour for which the formulation is developed. Our goal is to make the tangent of the curve at any point vary from the tangent of the initial
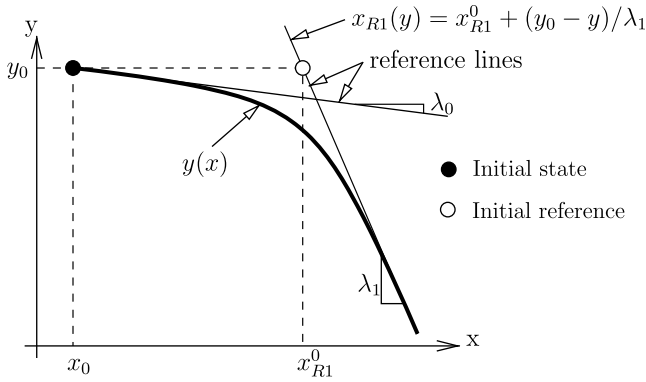
Fig. 4. Modelling using two references.

reference line (λ_0) to the tangent of the final reference (λ_1), as x increases. Thus, the current tangent is defined as

$$\frac{dy}{dx} = -\overline{\lambda} \tag{1}$$

where $\overline{\lambda}$ denotes a positive number and is defined in order to satisfy the requirement of smooth transition by means of

$$\overline{\lambda} = \lambda_0 + (\lambda_1 - \lambda_0)e^{-\overline{\beta}\overline{D}} \tag{2}$$

where $\overline{D}$ is the distance from the current state to the reference point x_{R1} located on the reference line with inclination equal to λ_1 (Fig. 4). This distance is defined as follows

$$\overline{D} = x_{R1}(y) - x \tag{3}$$

where x and y indicate the current state and x_{R1} is the x value for the same y state, however, located on the reference line. x_{R1} can be interpreted as an internal variable and can be easily obtained from

$$x_{R1}(y) = x_{R1}^0 + \frac{y_0 - y}{\lambda_1} \tag{4}$$

The exponential expression defined in Eq. (2) and illustrated in Fig. 5 yields a smooth transition where the current inclination $\overline{\lambda}$ is approximate equal to λ_0 when $\overline{D}$ is large and
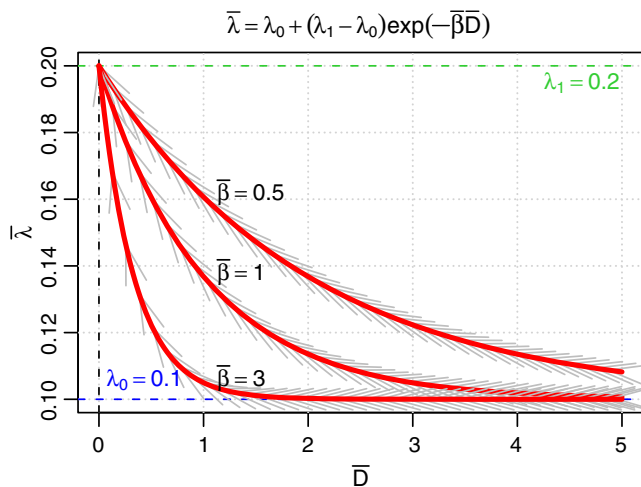
approaches λ_1 when $\overline{D}$ becomes zero. In this last case, the current state $\{x, y\}$ will coincide with the reference point $\{x_{R1}, y\}$. Note that $\overline{D}$ is always non-negative as we assumed that x approaches x_{R1} from the left side so that $x \leqslant x_{R1}$.

The speed of the transition is controlled by the $\overline{\beta}$ parameter. When $\overline{\beta}$ is small, the transition is smooth while when $\overline{\beta}$ is large, the curve follows a bilinear shape in which a discrete behaviour is predicted; however, the continuity is still preserved. For higher values of $\overline{\beta}$, the discrete model with inclinations λ_0 and λ_1 is very much approached. Therefore, the smooth model can be viewed as a general case for the bilinear model. In addition, this bilinear model, for example, the one defined by the Cam clay model using the inclinations of the NCL and URL, serves as reference for the parameter determination of the smooth curve.

Substituting Eq. (4) into Eq. (3), the result into Eq. (2) and then the last result into Eq. (1), an ordinary differential equation is obtained. This equation can be analytically integrated, as demonstrated in Appendix A, yielding the following solution

$$y(x) = -\lambda_0 x - \frac{\lambda_1}{\overline{\beta}}\ln(c_3 + c_2 e^{c_1 x}) \tag{5}$$

where c_1, c_2 and c_3 are functions of the constitutive parameters and initial values. These constants can be calculated using the reference inclinations and initial internal variables as follows

$$c_1 = \overline{\beta}(1 - \lambda_0/\lambda_1), \quad c_2 = e^{-\overline{\beta}(x_{R1}^0 + y_0/\lambda_1)} \quad \text{and}$$
$$c_3 = e^{-\overline{\beta}(y_0 + \lambda_0 x_0)/\lambda_1} - c_2 e^{c_1 x_0} \tag{6}$$

The value of $\overline{\beta}$ can be determined from experimental data through an energy equivalence approach by equating the area below the analytical $y(x)$ curve to that computed from experimental data. In this way, as deduced in Appendix A, the area below the analytical curve can be obtained by the following expression

$$S(x) = \int y(x)dx = \frac{-\lambda_0}{2}x^2 - \frac{\lambda_1}{\overline{\beta}}L(x) \tag{7}$$

where $L(x)$ is a function of the constants c_1, c_2, and c_3 and is given by Eq. (50) of Appendix A

3.2. Three references – Case 1

Three reference lines are considered when the curve $y(x)$ has a sigmoid shape, as shown in Fig. 6. By using two of these lines, with inclinations λ_1 and λ_2, a *reference curve* can be defined. This reference curve can be obtained by a procedure analogous to the one presented in the previous section. A variable tangent ($\overline{\overline{\lambda}}$) to the curve $y(x)$ is then adopted as a function of the inclination of the first reference line (λ_0) and the current inclination ($\overline{\lambda}$) of the reference curve. This function ($\overline{\overline{\lambda}}$) depends on the current state $\{x, y\}$ and a reference point $\{x_{R1}, y\}$ on the reference curve. This recursive approach is simple yet powerful for the simulation of complicated behaviour of geo-materials.
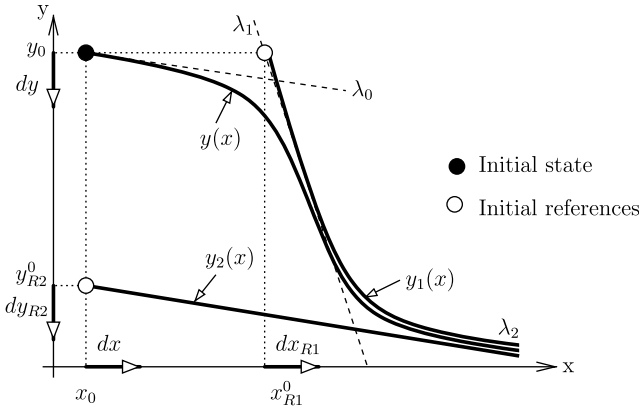

Fig. 5. Variation of $\overline{\lambda}$ with respect to the distance $\overline{D}$.

Fig. 6. Modelling using three references – case 1.

The reference curve, indicated by $y_1(x)$ in Fig. 6, is controlled by λ_1 and λ_2 and can be obtained in an analogous way as for the two references case presented in the previous section. The current tangent inclination to this curve is defined by

$$\frac{dy_1}{dx} = -\overline{\lambda} \tag{8}$$

where $\overline{\lambda}$ is given by

$$\overline{\lambda} = \lambda_1 + (\lambda_2 - \lambda_1)e^{-\overline{\beta D}} \tag{9}$$

and the *vertical distance* is defined as follows (Fig. 6):

$$\overline{D} = y - y_{R2}(x) \tag{10}$$

where y_{R2} is the ordinate of the reference line with inclination equal to λ_2, and, for the current state $\{x,y\}$, it can be calculated by

$$y_{R2}(x) = y_{R2}^0 - \lambda_2(x - x_0) \tag{11}$$

The deduction presented in Appendix A can then be applied to Eqs. (8)–(11) in order to obtain an analytical expression for the reference curve. This yields:

$$y_1(x) = -\lambda_1 x + \frac{1}{\overline{\beta}} \ln(c_3 + c_2 e^{c_1 x}) \tag{12}$$

where the constants c_1, c_2, and c_3 are given by

$$c_1 = \overline{\beta}(\lambda_1 - \lambda_2), \quad c_2 = e^{\overline{\beta}(y_{R2}^0 + \lambda_2 x_0)} \quad \text{and}$$
$$c_3 = e^{\overline{\beta}(y_0 + \lambda_1 x_{R1}^0)} - c_2 e^{c_1 x_{R1}^0} \tag{13}$$

The area below this reference curve can be calculated with the aid of the following equation:

$$S_1(x) = \int y_1(x)dx - \frac{\lambda_1}{2}x^2 + \frac{1}{\overline{\beta}}L(x) \tag{14}$$

which is useful for the determination of the $\overline{\beta}$ parameter.

Now, the tangent inclination to the $y(x)$ curve can be defined by means of

$$\frac{dy}{dx} = -\overline{\overline{\lambda}} \tag{15}$$

where

$$\overline{\overline{\lambda}} = \lambda_0 + (\overline{\lambda} - \lambda_0)e^{-\overline{\overline{\beta D}}} \tag{16}$$

is a function of the inclination $\overline{\lambda}$ and of the following *horizontal distance* from the current state $\{x,y\}$ to a point $\{x_{R1},y\}$ on the reference curve y_1

$$\overline{\overline{D}} = x_{R1} - x \tag{17}$$

When $\overline{\overline{D}}$ is large, the inclination $\overline{\overline{\lambda}}$ is close to λ_0. Conversely, when $\overline{\overline{D}} \to 0$, $\overline{\overline{\lambda}}$ is close to $\overline{\lambda}$, i.e., the current tangent inclination of $y(x)$ curve will be equal to the current tangent inclination of y_1 curve. If $\overline{\beta} \to \infty$ and $\overline{\overline{\beta}} \to \infty$, the sigmoid-shaped curve $y(x)$ will be similar to a tri-linear model using λ_0, λ_1 and λ_2.

From Eq. (12) it is difficult to find x_{R1} as a function of the current y state. However, x_{R1} can be understood as an internal variable and, together with the current state, be used for the representation of the non-linear behaviour predicted. In addition, its evolution, given by

$$\frac{dx_{R1}}{dy} = \frac{-1}{\overline{\lambda}} \tag{18}$$

must be integrated at the same time as the evolution of the current state (Eq. (15)).

3.2.1. Incremental relation

For convenience, vector notation is employed in the following expressions. The current state is represented by the pair

$$x \quad \text{and} \quad E = \left\{ \begin{array}{c} y \\ x_{R1} \end{array} \right\} \tag{19}$$

when x is the driver variable, and by the pair

$$y \quad \text{and} \quad S = \left\{ \begin{array}{c} x \\ x_{R1} \end{array} \right\} \tag{20}$$

when y is the driver variable. The non-linear incremental relation can thus be symbolised as

$$dE = C(x,E)dx = C(x,y,x_{R1})dx \tag{21}$$

or, alternatively,

$$dS = D(y,S)dy = D(y,x,x_{R1})dy \tag{22}$$

where the tangent modulus C (analogous to the "Compliance") and D (analogous to the "Stiffness") were defined. From Eqs. (15) and (18) these moduli can be written as follows

$$C = \frac{dE}{dx} = \left[\begin{array}{c} -\overline{\overline{\lambda}} \\ \overline{\overline{\lambda}}/\overline{\lambda} \end{array} \right] \Rightarrow dE = \left\{ \begin{array}{c} dy \\ dx_{R1} \end{array} \right\} = \left[\begin{array}{c} -\overline{\overline{\lambda}} \\ \overline{\overline{\lambda}}/\overline{\lambda} \end{array} \right] dx \tag{23}$$

and

$$D = \frac{dS}{dy} = \left[\begin{array}{c} -1/\overline{\overline{\lambda}} \\ -1/\overline{\lambda} \end{array} \right] \Rightarrow dS = \left\{ \begin{array}{c} dx \\ dx_{R1} \end{array} \right\} = \left[\begin{array}{c} -1/\overline{\overline{\lambda}} \\ -1/\overline{\lambda} \end{array} \right] dy \tag{24}$$

for which any ODE solver, such as the ones based on the Runge–Kutta method, can be applied during a numerical integration in order to solve Eqs. (21) or (22).

3.3. Three references – Case 2

This case, illustrated in Fig. 7, is equivalent to the previous one. The only difference is that only *horizontal* distances ($\overline{D}$ and $\overline{\overline{D}}$) are considered. x_{R1} is now located on the reference line with an inclination equal to λ_1 and a new internal variable x_{R3}, located on the *reference curve* y_3, is employed. The reference curve y_3 is controlled by the two inclinations λ_3 and λ_1. Eqs. (15) and (16) for dy/dx and $\overline{\overline{\lambda}}$, respectively, are still valid; however, the distance $\overline{\overline{D}}$ is now given by

$$\overline{\overline{D}} = x_{R3} - x \tag{25}$$

The reference curve now has inclination defined by

$$\frac{dy_3}{dx} = -\overline{\lambda} \tag{26}$$

where

$$\overline{\lambda} = \lambda_3 + (\lambda_1 - \lambda_3)e^{-\overline{\beta}\overline{D}} \tag{27}$$

begins from λ_3 and goes to λ_1, as the *horizontal distance* $\overline{D}$ decreases. This distance is given by

$$\overline{D} = x_{R3} - x_{R1}(y) \tag{28}$$

where x_{R3} is the abscissa on the y_3 curve for the current y state and x_{R1} can be calculated by

$$x_{R1}(y) = x_{R1}^0 + \frac{y_0 - y}{\lambda_1} \tag{29}$$

Again, considering the general form presented in Appendix A, the four Eqs. (26)–(29) lead to the following analytical solution for the reference curve

$$y_3(x) = -\lambda_3 x + \frac{\lambda_1}{\overline{\beta}} \ln(c_3 + c_2 e^{c_1 x}) \tag{30}$$

where the constants are given by

$$c_1 = \overline{\beta}(\lambda_3/\lambda_1 - 1), \quad c_2 = e^{\overline{\beta}(x_{R1}^0 + y_0/\lambda_1)} \quad \text{and}$$
$$c_3 = e^{\overline{\beta}(y_0 + \lambda_3 x_{R3}^0)/\lambda_1} - c_2 e^{c_1 x} \tag{31}$$

Likewise, the $\overline{\beta}$ parameter can be determined by correlating the area below y_3 curve with the area computed from experimental data. This area can be calculated by the following expression
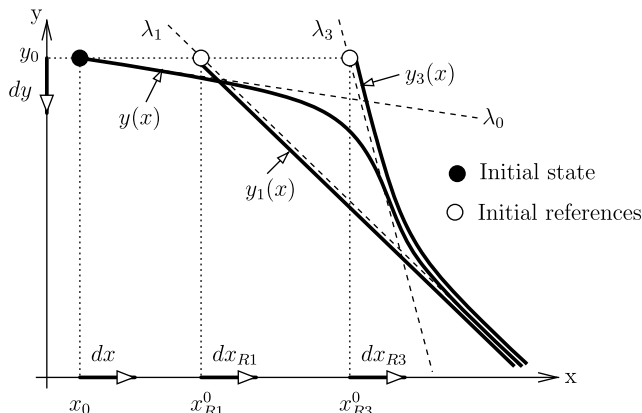

Fig. 7. Modelling using three references – case 2.

$$S_3(x) = \int y_3(x)dx = \frac{-\lambda_3}{2}x^2 + \frac{\lambda_1}{\overline{\beta}}L(x) \tag{32}$$

3.3.1. Incremental relation

Using similar vectorial notations as before, the non-linear incremental relation can be expressed as

$$dE = C(x, E)dx = C(x, y, x_{R3})dx \tag{33}$$

or

$$dS = D(y, S)dy = D(y, x, x_{R3})dy \tag{34}$$

where

$$C = \frac{dE}{dx} = \begin{bmatrix} -\overline{\overline{\lambda}} \\ \overline{\overline{\lambda}}/\overline{\lambda} \end{bmatrix} \Rightarrow dE = \left\{ \begin{array}{c} dy \\ dx_{R3} \end{array} \right\} = \begin{bmatrix} -\overline{\overline{\lambda}} \\ \overline{\overline{\lambda}}/\overline{\lambda} \end{bmatrix} dx \tag{35}$$

and

$$D = \frac{dS}{dy} = \begin{bmatrix} -1/\overline{\overline{\lambda}} \\ -1/\overline{\lambda} \end{bmatrix} \Rightarrow dS = \left\{ \begin{array}{c} dx \\ dx_{R3} \end{array} \right\} = \begin{bmatrix} -1/\overline{\overline{\lambda}} \\ -1/\overline{\lambda} \end{bmatrix} dy \tag{36}$$

i.e., the only difference is the substitution of x_{R1} by x_{R3}.

3.4. Summary

Table 1 presents conveniently all equations for the three set of formulae based on the "reference curves". Appendix B presents the computer codes for the "R Project for Statistical Computing" software [13] based on these equations and that were used for the numerical simulations.

4. Stress–strain and water retention relationships

The non-linear stress–strain relationship can be directly deduced from

$$\frac{dy}{dx} = -\overline{\lambda}(x, y, r) \quad \text{or} \quad \frac{dy}{dx} = -\overline{\overline{\lambda}}(x, y, r) \tag{37}$$

where "r" stands for the internal variable (reference) considered. For example, if

$$y = e \quad \text{and} \quad x = \ln p \tag{38}$$

where e is the void ratio and p the mean effective stress, then

$$de = dy = \frac{dy}{dx}\frac{dx}{dp}dp = -\overline{\lambda}\frac{dp}{p} \tag{39}$$

Therefore, the stress–strain relationship is given by

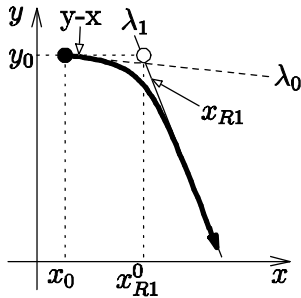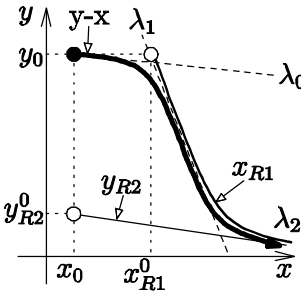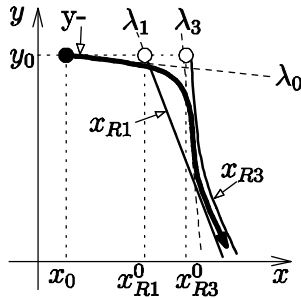$$d\varepsilon_v = \frac{\overline{\lambda}(p, e)}{1 + e}\frac{dp}{p} \tag{40}$$

where

$$d\varepsilon_v = \frac{-dv}{v} = \frac{-de}{1 + e} \tag{41}$$

and v is the specific volume.

Alternatively, if, for example,

Table 1
Summary of all equations based on the "reference concept"

First reference	$x_{R1}(y) = x_{R1}^0 + \frac{1}{\lambda_1}(y_0 - y)$	$y_{R2}(x) = y_{R2}^0 - \lambda_2(x - x_0)$	$x_{R1}(y) = x_{R1}^0 + \frac{1}{\lambda_1}(y_0 - y)$
Second reference		x_{R1}	x_{R3}
First distance	$\overline{D} = x_{R1} - x$	$\overline{D} = y - y_{R2}(x)$	$\overline{D} = x_{R3} - x_{R1}(y)$
Second distance		$\overline{\overline{D}} = x_{R1} - x$	$\overline{\overline{D}} = x_{R3} - x$
First inclination	$\overline{\lambda} = \lambda_0 + (\lambda_1 - \lambda_0)e^{-\overline{\beta}\overline{D}}$	$\overline{\lambda} = \lambda_1 + (\lambda_2 - \lambda_1)e^{-\overline{\beta}\overline{D}}$	$\overline{\lambda} = \lambda_3 + (\lambda_1 - \lambda_3)e^{-\overline{\beta}\overline{D}}$
Second inclination		$\overline{\overline{\lambda}} = \lambda_0 + (\overline{\lambda} - \lambda_0)e^{-\overline{\overline{\beta}}\,\overline{\overline{D}}}$	$\overline{\overline{\lambda}} = \lambda_0 + (\overline{\lambda} - \lambda_0)e^{-\overline{\overline{\beta}}\,\overline{\overline{D}}}$
Incremental relation		$\begin{Bmatrix} dx \\ dx_{R1} \end{Bmatrix} = \begin{bmatrix} -1/\overline{\overline{\lambda}} \\ -1/\overline{\lambda} \end{bmatrix} dy$ $\begin{Bmatrix} dy \\ dx_{R1} \end{Bmatrix} = \begin{bmatrix} -\overline{\overline{\lambda}} \\ \overline{\overline{\lambda}}/\overline{\lambda} \end{bmatrix} dx$	$\begin{Bmatrix} dx \\ dx_{R3} \end{Bmatrix} = \begin{bmatrix} -1/\overline{\overline{\lambda}} \\ -1/\overline{\lambda} \end{bmatrix} dy$ $\begin{Bmatrix} dy \\ dx_{R3} \end{Bmatrix} = \begin{bmatrix} -\overline{\overline{\lambda}} \\ \overline{\overline{\lambda}}/\overline{\lambda} \end{bmatrix} dx$
Analytical solutions	$c_1 = \overline{\beta}(1 - \lambda_0/\lambda_1)$	$c_1 = \overline{\beta}(\lambda_1 - \lambda_2)$	$c_1 = \overline{\beta}(\lambda_3/\lambda_1 - 1)$
	$c_2 = e^{-\overline{\beta}(x_{R1}^0 + y_0/\lambda_1)}$	$c_2 = e^{\overline{\beta}(y_{R2}^0 + \lambda_2 x_0)}$	$c_2 = e^{\overline{\beta}(x_{R1}^0 + y_0/\lambda_1)}$
	$c_3 = e^{-\overline{\beta}(y_0 + \lambda_0 x_0)/\lambda_1} - c_2 e^{c_1 x_0}$	$c_3 = e^{\overline{\beta}(y_0 + \lambda_1 x_{R1}^0)} - c_2 e^{c_1 x_{R1}^0}$	$c_3 = e^{\overline{\beta}(y_0 + \lambda_3 x_{R3}^0)/\lambda_1} - c_2 e^{c_1 x}$
	$y = -\lambda_0 x - \frac{\lambda_1}{\overline{\beta}} \ln(c_3 + c_2 e^{c_1 x})$	$y_1 = -\lambda_1 x + \frac{1}{\overline{\beta}} \ln(c_3 + c_2 e^{c_1 x})$	$y_3 = -\lambda_3 x + \frac{\lambda_1}{\overline{\beta}} \ln(c_3 + c_2 e^{c_1 x})$
	$S = \frac{-\lambda_0}{2} x^2 - \frac{\lambda_1}{\overline{\beta}} L(x)$	$S_1 = \frac{-\lambda_1}{2} x^2 + \frac{1}{\overline{\beta}} L(x)$	$S_3 = \frac{-\lambda_3}{2} x^2 + \frac{\lambda_1}{\overline{\beta}} L(x)$
Auxiliary function	$L(x) = x\ln(c_3 + c_2 e^{c_1 x}) - x\ln\left(1 + \frac{c_2}{c_3} e^{c_1 x}\right) - \frac{1}{c_1} \mathrm{li}_2\left(\frac{-c_2}{c_3} e^{c_1 x}\right)$		

$$y = \ln v \quad \text{and} \quad x = \ln p \tag{42}$$

then

$$dv = v\,dy = v\frac{dy}{dx}\frac{dx}{dp}dp = -v\overline{\lambda}\frac{dp}{p} \tag{43}$$

and, therefore,

$$d\varepsilon_v = \overline{\lambda}(p, v)\frac{dp}{p} \tag{44}$$

For the saturation–suction relation, if,

$$y = Sr \quad \text{and} \quad x = \ln s \tag{45}$$

then,

$$dSr = \frac{dSr}{ds}ds = \frac{dSr}{dx}\frac{dx}{ds}ds = \frac{dy}{dx}\frac{dx}{ds}ds = \frac{-\overline{\overline{\lambda}}(s, Sr, r)}{s}ds \tag{46}$$

Likewise, when $y = \theta_w$, an expression similar to Eq. (46) is found, changing Sr by θ_w.

Therefore, the incorporation of the "reference concept" in a constitutive model is straightforward, considering the tangent modulus given by Eqs. (40) or (46), for example.

5. Applications

In this section, we illustrate the application of the equations proposed to different problems in soil mechanics. These include two isotropic compression tests on sands, saturation–suction tests on the Hostun sand and a silty clay, a water content–suction test on a geotextile, and four tests on three natural clays and a structured calcarenite. The determination of parameters is explained in detail for all these tests.

5.1. Isotropic compression of sands

Two isotropic compression tests are studied in this section. They were carried out for Sacramento River sand and presented in Lee and Seed [6] and for Cambria sand as presented by Lade and Bopp [4]. All parameters were obtained directly from e–$\ln p'$ or e–$\ln \sigma_3'$ plots and are summarized in Tables 2 and 3. The determination of these parameters is explained as follows.

As illustrated in Fig. 8 for the Sacramento River sand, a reference line with inclination λ_0 was selected from the first point on the curve with the highest initial void ratio. In order to find λ_1 inclination, the following procedure was adopted: (1) the four data curves for the four different initial void ratios were extended to a further point with higher mean pressure where these curves are close enough one from each other; and (2) a line passing by this final point and almost touching the data points was selected. The inclination λ_1 is the inclination of this last line.

This procedure is related to the idea of a limit compression line (LCL), in the view that the line with λ_1 inclination should be parallel to the LCL. Certainly this procedure is a little subjective; nonetheless, this technique is quite common in other engineering practices, for example, in the procedure to find the pre-consolidation stress for over consolidated clays (see for example [1]). Moreover, the equations proposed are flexible enough to allow slight differences on these inclinations. This feature allows great robustness for the simulation of the complicate mechanical behaviour even for highly non-linear relations.

The same procedures were applied for the determination of the λ_0 and λ_1 parameters of Cambria sand (Fig. 9). However, due to the availability of more data points on the compression curves, a better (easier) estimate of λ_1 could be obtained. In this case, the last points on all curves were used to fix the λ_1 line. Afterwards, as for the Sacramento River sand, all initial internal variables σ_3^0 or p_0' could be determined. These variables, represented by x_{R1}^0, can be directly calculated considering the common point at the
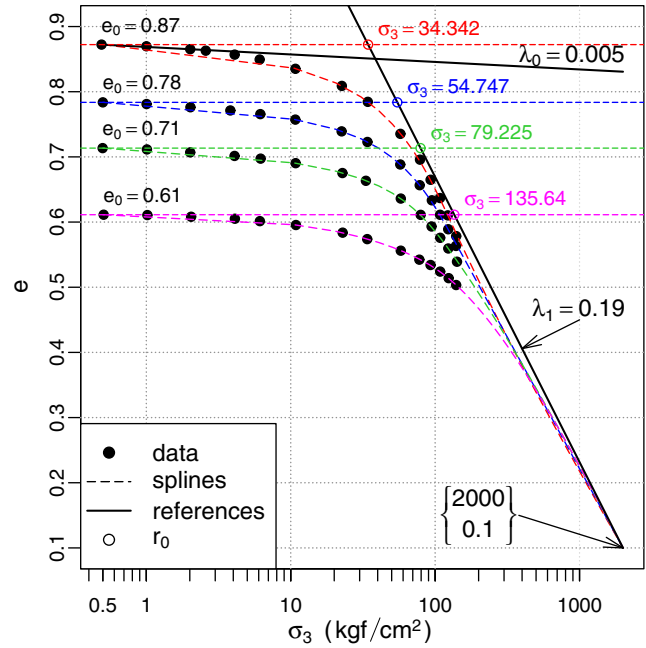

Fig. 8. Isotropic compression behaviour of Sacramento River sand (data after [6]).
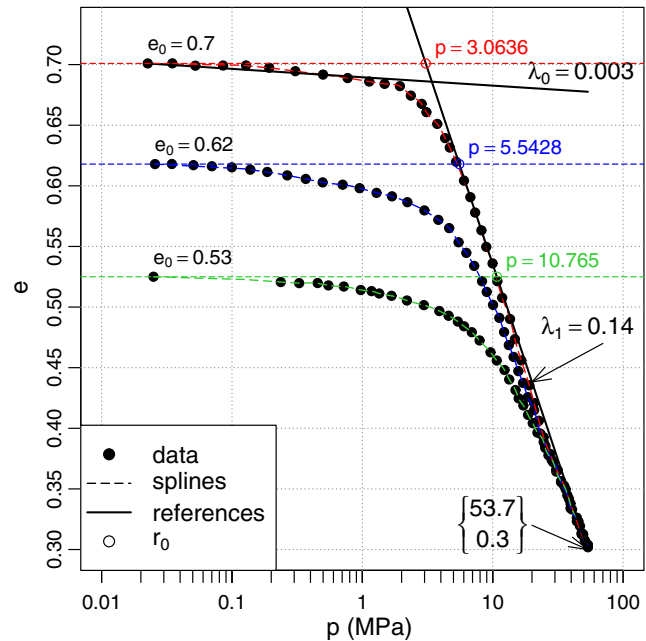

Fig. 9. Isotropic compression behaviour of Cambria sand (data after [4]).

end (higher pressures) of all extrapolated curves and the LCL line with inclination equal to λ_1.

The $\overline{\beta}$ parameters related to the curvature of each curve were determined by comparing the area below the data curves with the analytical solution provided by Eq. (7). Compared to the $\overline{\beta}$ values for Sacramento River sand, the values of $\overline{\beta}$ for Cambria sand computed for each curve with different initial void ratios differ more significantly from each other. For example, the curve with $e_0 = 0.7$ for

Table 2
Parameters and initial conditions for Sacramento River sand

Variables and units	e_0	σ_3^0	$\exp x_{R1}^0$	λ_0	λ_1	$\overline{\beta}$
$y = e$, $x = \ln \sigma_3$ (kgf/cm^2)	0.87	0.5	34.3	0.005	0.19	1.55
	0.78	0.5	54.7			
	0.71	0.5	79.2			
	0.61	0.5	135.6			

Table 3
Parameters and initial conditions for Cambria sand

Variables and units	e_0	p_0	$\exp x_{R1}^0$	λ_0	λ_1	$\overline{\beta}$
$y = e$, $x = \ln p$ (MPa)	0.70	0.02	3.1	0.003	0.14	2.28
	0.62	0.02	5.5			
	0.53	0.2	10.8			

Cambria sand has a higher curvature than the curve with $e_0 = 0.53$. However, an average value of $\overline{\beta}$ was selected considering all curves with different initial void ratios. These values are presented in Tables 2 and 3. The computer codes used to find them and which are quite convenient are explained in Appendix B.

Fig. 10 presents the simulations using the equations proposed for the Sacramento River sand with different initial values. The continuous lines were computed considering only one sequence of data points; therefore, they are the best fit for each curve with different initial void ratio. The dashed lines were calculated using the parameters obtained (averaged) and considering each different initial void ratios. It can be observed that the simulated curves (dashed) are slightly different from the predicted curves (continuous). The difference is due to the averaged $\overline{\beta}$ parameter selected. A better fit could be obtained if a correlation between $\overline{\beta}$ and the initial void ratio was introduced. However, this would require the substitution of $\overline{\beta}$ with another parameter relating initial values with curvatures. This extension is left for a future study.

The simulations for Cambria sand with different initial states are illustrated by the dashed lines in Fig. 11. As discussed before, due to the differences on each $\overline{\beta}$ parameter determined for each data curve, the simulations with an averaged $\overline{\beta}$ value are slightly different from the predictions (continuous lines) for each data series.

From Figs. 10 and 11 it is possible to conclude that the "reference curves" concept allows the definition of equations that are at the same time versatile, robust and reasonably accurate for the simulation of the isotropic compression of the Sacramento River and Cambria sands.

5.2. Water retention characteristics

The phenomenon observed from the water retention can be represented by the same equations deduced from the "reference curves" concept since the curves drawn for the degree of saturation or water content *versus* suction state variables have the same shape as the non-linear void ratio–mean stress curves. The formulations given by Eqs. (21) and (22) for the three-references – case 1 are used in this case. Three sets of experiments on three different materials are considered: (1) tests on a sample of Hostun sand as presented by Lins et al. [7]; (2) tests on a silty clay as presented by Cunningham et al. [2]; and (3) tests on a geotextile as presented by Nahlawi et al. [9]. All parameters were obtained directly from the experimental results. These are summarized in Table 4.
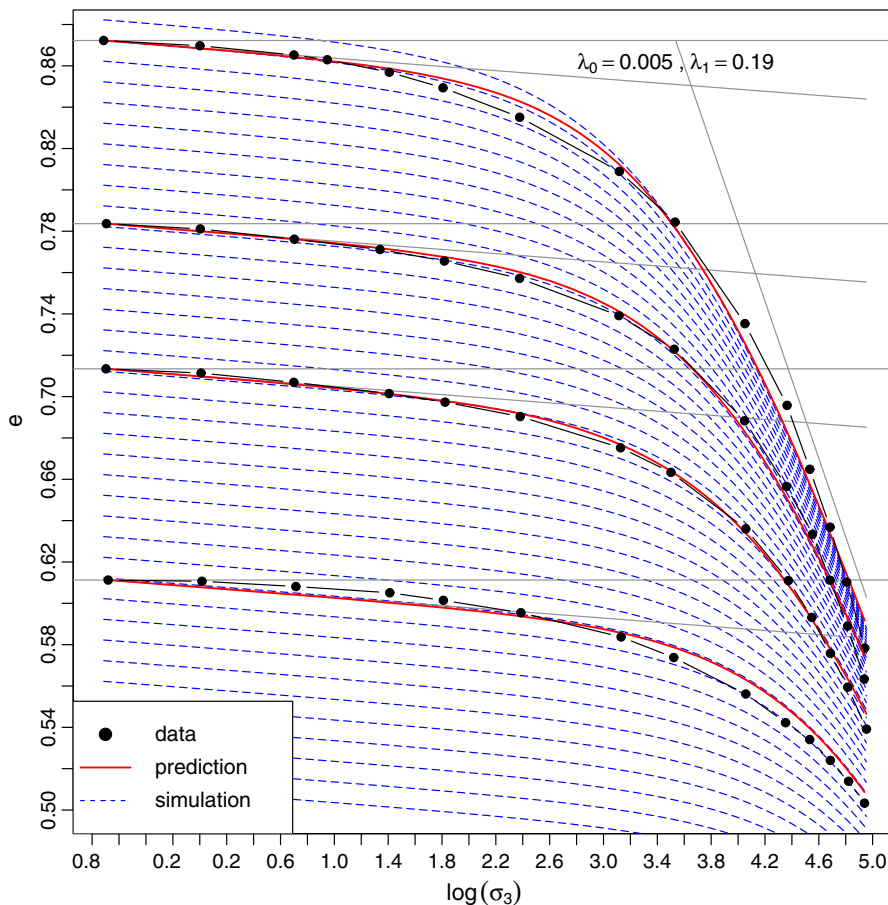

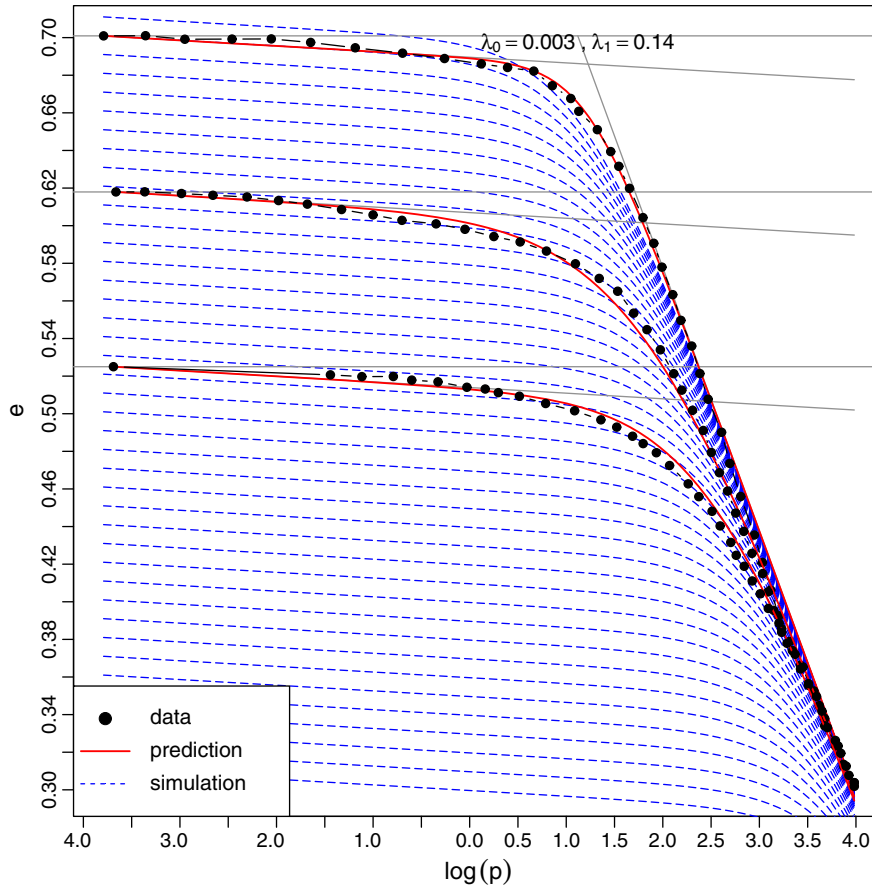Fig. 10. Predictions of the isotropic behaviour of Sacramento River sand.

Fig. 11. Predictions of isotropic behaviour of Cambria sand.

Table 4
Parameters and initial values for the three water retention curves

Material	x_0	y_0	x_{R1}^0	y_{R2}^0	λ_0	λ_1	λ_2	$\bar{\bar{\beta}}$	$\bar{\beta}$
Hostun sand ($x_0 = \ln s_0$, $y_0 = Sr^0$)	−2.30	1.0	0.365	0.109	0.01	1.7	0.011	9.755	3.335
Silty clay ($x_0 = \ln s_0$, $y_0 = Sr^0$)	2.57	1.0	6.1	0.139	0.0	0.45	0.01	4.532	3.974
Geotextile ($x_0 = \ln s_0$, $y_0 = \theta_w^0$)	−2.30	0.882	0.191	0.169	0.0	1.33	0.02	5.023	9.452

Fig. 12 shows the experimental results and predictions for the Hostun sand. The three parameters λ_0, λ_1, and λ_2 were found simply by considering some points on each section of the curve with different main inclination. The two or three initial data points were fitted by a line with inclination equal to λ_0. Likewise, some points on the drying section with higher gradient were used to find λ_1. Finally, the last points with higher suction values were used to find λ_2. The same procedure was used in order to find the three inclinations for the Sr–$\ln s$ curve of the silty clay (Fig. 13) and the θ_w–$\ln s$ curve of the geotextile (Fig. 14).

The initial internal variables x_{R1} can be found considering an inflection point around the mid portion on each experimental curve of Figs. 12–14. These variables, summarized in Table 4, were calculated for the reference line with inclination equal to λ_1. Afterwards, the curvature of the end portion of these curves, represented by the $\bar{\beta}$ parameter, could be obtained by comparing the analytical and experimental areas below the curve from the inflection

point to the end (higher suction values) of each curve (see Fig. 20 in Appendix B). The analytical area is calculated using Eq. (14) for the three-references – case 1.

The curvature $\bar{\bar{\beta}}$ of the initial portion of each curve shown in Figs. 12–14 can be directly obtained considering the curve from the points with lower suction values to the inflection point as a "two references" model. In this case, only λ_0 and λ_1 are considered and Eq. (7) is used to find the analytical area. Therefore, both $\bar{\bar{\beta}}$ and $\bar{\beta}$ parameters can be automatically computed using the function "find.betas" of Appendix B. The inputs for this function are the inclinations λ_0, λ_1, and λ_2, the inflection point, and the data values stored into two arrays Xd and Yd (see Appendix B for more details).

The continuous curves drawn in Figs. 12–14 express the results using Eq. (23). Alternatively, these results could be obtained using Eq. (36). The solution is obtained by a numerical integration scheme such as the Runge–Kutta method. The initial state, including initial internal variables
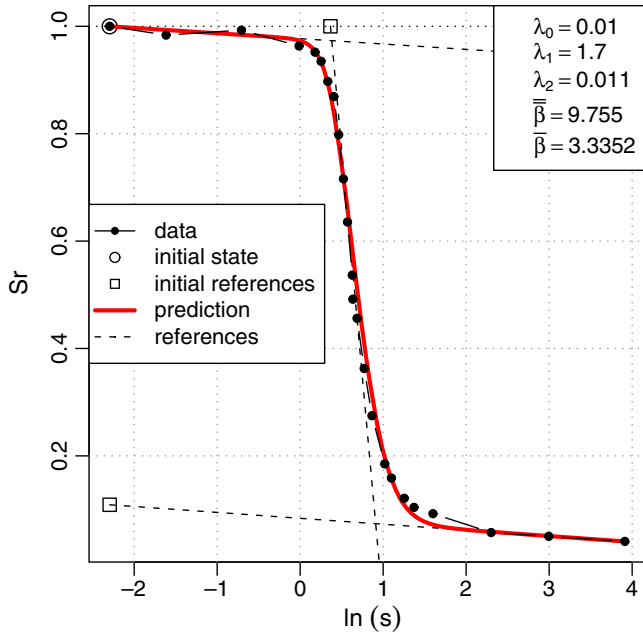
Fig. 12. Predictions and experimental observations of the saturation–suction of Hostun sand (data after [7]).

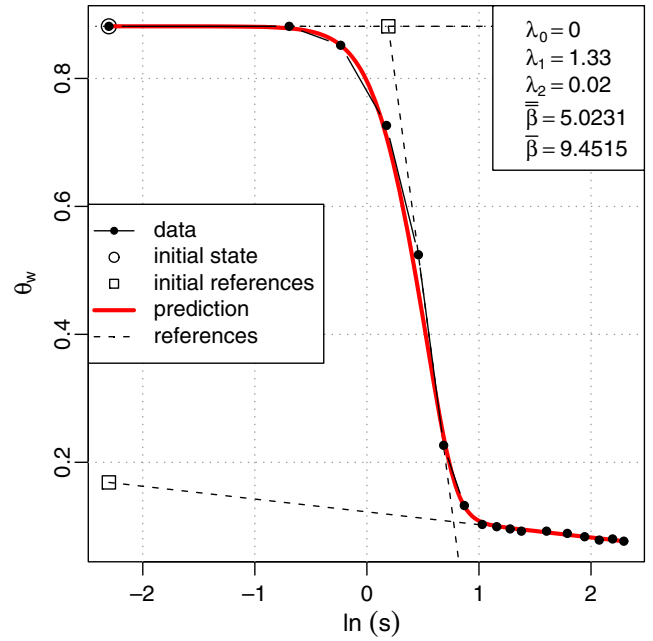

Fig. 14. Predictions and experimental observations of a geotextile (data after [9])
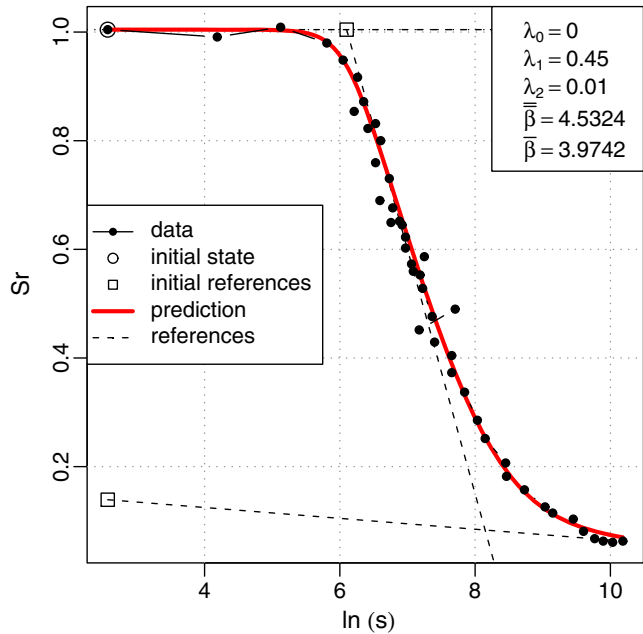

Fig. 13. Predictions and experimental observations of a silty clay (data after [2]).

as illustrated in Figs. 12–14, has been considered during the numerical simulations. From the figures, it can be concluded that the numerical prediction coincides with the experimental results very well.

5.3. Volumetric behaviour of structured materials

In this section, four experimental tests on structured materials are considered for the verification of the formulations proposed: (1) tests on Leda clay as discussed in Liu and Carter [8]; (2) tests on a structured calcarenite presented by Lagioia and Nova [5]; (3) tests on Osaka clay presented by Nakano et al. [10]; and (4) tests on Joetsu clay also presented by Nakano et al. [10]. Again, all parameters were obtained directly from the experimental curves and are summarized in Table 5.

The results with Leda clay (Fig. 15) and the structured calcarenite (Fig. 16) both exhibit a sigmoid curve in the v–$\ln \sigma'_v$ or v–$\ln p'$ planes. The final portion (higher pressures) of these curves reaches the normal consolidation line (NCL), which has an inclination equal to λ_1. Therefore, we can follow the same procedure as for the water retention curves of the previous section in order to find the parameters for these tests. In this case, the initial internal variables

Table 5
Parameters and initial values for the four tests on structured materials

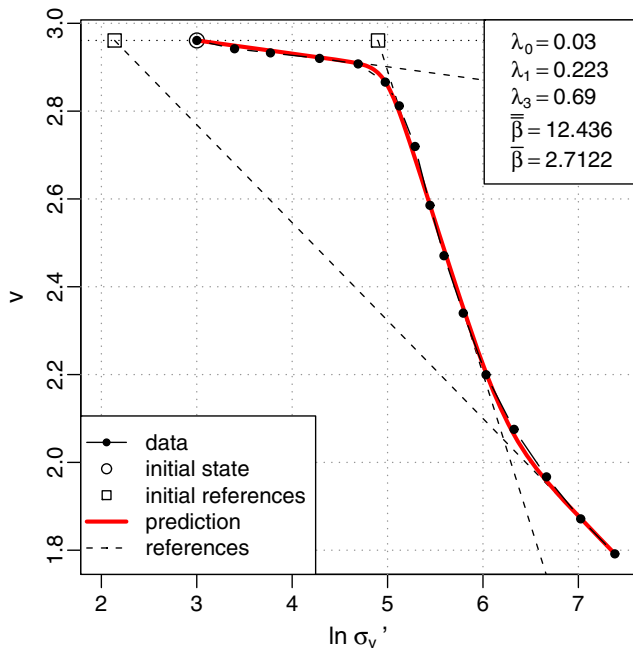| Material	x_0	y_0	x_{R1}^0	x_{R3}^0	λ_0	λ_1	λ_3	$\bar{\bar{\beta}}$	$\bar{\beta}$
Leda clay ($x_0 = \ln \sigma_v^0$, $y_0 = v_0$)	3.0	2.96	2.14	4.9	0.03	0.223	0.69	12.44	2.712
Calcarenite ($x_0 = \ln p_0$, $y_0 = v_0$)	4.99	2.15	6.83	7.8	0.0165	0.208	3.0	20.0	4.0
Osaka clay ($x_0 = \ln p_0$, $y_0 = v_0$)	1.81	2.52	2.64	4.62	0.01	0.197	0.30	1.546	10.0
Joetsu clay ($x_0 = \ln p_0$, $y_0 = v_0$)	3.90	2.44	3.63	5.31	0.049	0.224	0.338	4.168	10.0

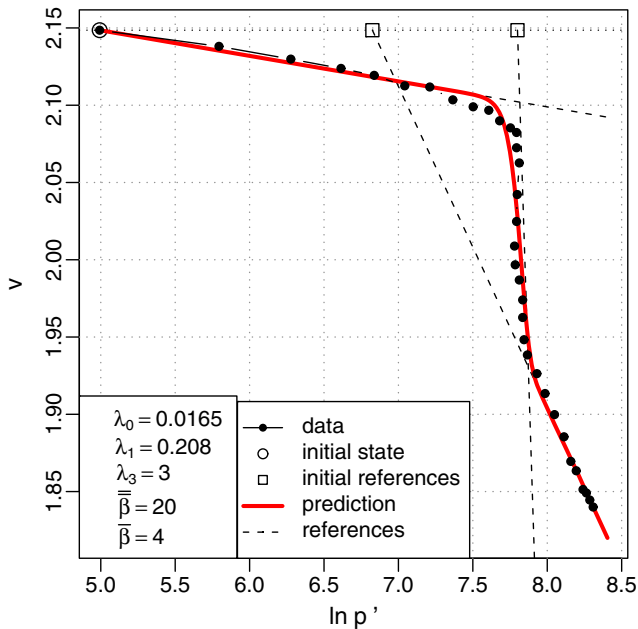Fig. 15. Predictions and experimental observations of the volumetric behaviour of Leda clay (data after [8]).

Fig. 16. Predictions and experimental observations of the volumetric behaviour of a structured calcarenite (data after [5]).

x_{R1}^0 and x_{R3}^0 must be set according to the current initial state represented by x_0 and y_0. These can be easily calculated considering the equations of the lines with inclinations λ_1 and λ_3.

For Leda clay, an inflection point, selected along the destructuration portion, was used to split the curve into two parts. The area of the first portion was used to find the value of $\overline{\overline{\beta}}$ and the second part for $\overline{\beta}$. The analytical

value of the area below the first portion is calculated using Eq. (7), in view that the first portion may be represented by a two references model with inclinations λ_0 and λ_3. The area for the final portion can be calculated with Eq. (32), for the three references – case 2.

For the calcarenite, however, the value of $\overline{\beta}$ was not automatically computed and was fixed equal to 4.0 because the numerical integration failed sometimes due to the high value selected for the gradient $\lambda_3 = 3.0$. In addition, for the calcarenite, $\overline{\overline{\beta}}$ was adopted equal to 20.0 in the view that a higher value of this parameter would make the predicted curve approach the bilinear model with inclinations λ_0 and λ_3. Therefore, although the calibration in this case was made by directly adjusting the predicted curve to the data points, a straightforward procedure was available due to the main feature of the "reference curves" concept where the reference lines always serve as a guide for the range of β parameters, as larger values will make the smooth curve approach the bilinear model.

From Figs. 15 and 16, we can observe that the calculations with the equations based on the "reference curves" concept are in good agreement with the experimental results.

Figs. 17 and 18 present the experimental results of compression tests on Osaka and Joetsu structured clays [10]. For each soil, two curves are presented: one for the same soil in a remoulded state; and the other for the structured material. For these tests, the last points for higher mean pressures do not reach the normal compression line because these testes were stopped before all structure was lost. Nonetheless, it is possible to observe that the structured line would approach the normal consolidation line
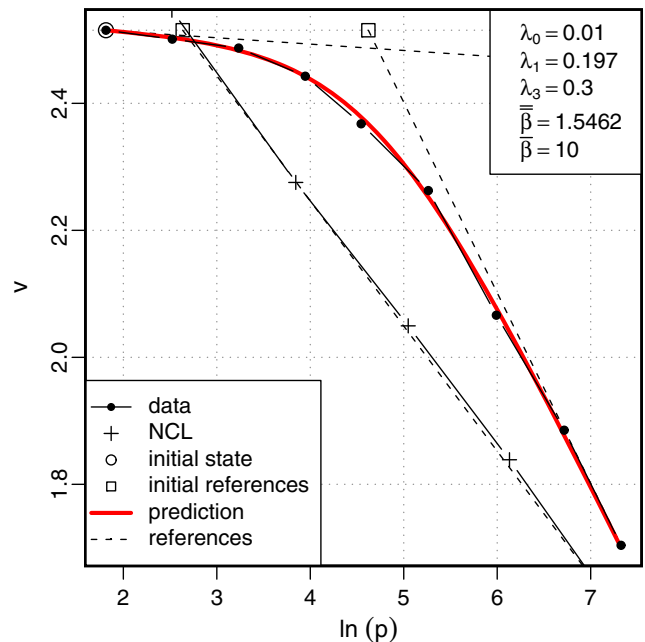

Fig. 17. Predictions and experimental observations of the volumetric behaviour of Osaka clay (data after [10]).
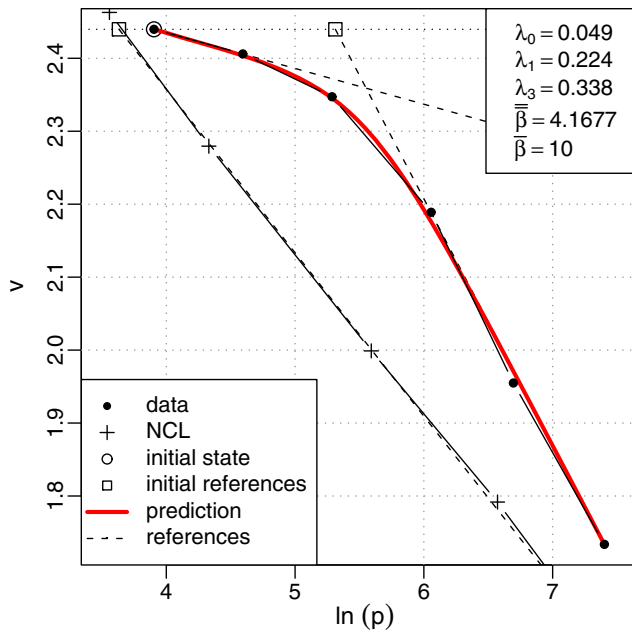
Fig. 18. Predictions and experimental observations of the volumetric behaviour of Joetsu clay (data after [10]).

if higher pressures were applied. The three reference inclinations λ_0 (initial), λ_1 (NCL) and λ_3 (structured) can be directly obtained from these data. The initial inclination (λ_0) was selected for some initial points on the data curve. The normal consolidation line inclination (λ_1) can be easily determined from experimental results on remoulded materials. For the inclination (λ_3) of the structured main response, the last points on the end portion of the structured curve were chosen in order to calculate λ_3. We note that this inclination can vary slightly if the tests were conducted to higher pressures. However, for the range under study, the values selected for λ_3 seemed to be appropriate.

The values of $\overline{\beta}$ parameter for Osaka and Joetsu clays were not calculated from the area comparison, because, clearly, there are not enough points (at higher pressures) to determine the curvature when the structured response convert into the normal (NCL) response. Therefore, these values were fixed equal to 10.0, which would lead to higher curvatures for the structured-NCL transition and, then, the $\overline{\overline{\beta}}$ parameter would not have influence on the shape of the predicted curve. In this way, $\overline{\beta}$ could be calculated directly using a two-references model with the aid of Eq. (7). The predicted curves (contiguous lines) are illustrated in Figs. 17 and 18, and, again, the simulations agreed very well with the experimental data.

6. Conclusions

Three set of equations were deduced considering a concept here referred to as "reference curves". These equations provide smooth transition from initial and final behaviours that are commonly represented by bilinear or trilinear models. A phenomenological approach is taken

in account in which a studied behaviour is observed macroscopically by means of experimental curves. These curves are defined for some state variables and are used in order to identify some key reference lines or curves. The reference curves may have any orientation on plots where the coordinates are the main state variables. In addition, these references may cross each other during the evolution of the state variables. Reference curves can be defined in a recursive manner, letting the inclination of a specific reference line vary with respect to other reference lines. Therefore, even complicate behaviours may be represented with this concept.

An incremental relationship with internal variables is deduced from this method and, thus, incremental constitutive models can easily incorporate the resulting equations. At most five constitutive parameters are required to set the model. Three parameters are directly determined from lines identified as references in plots with experimental results. The method that considers inclinations on characteristic plots is common in engineering practice, for example, as in the Cam clay model. The unloading–reloading line (URL), the normal consolidation line (NCL), the limit compression line (LCL), the initial or residual lines and the structured line, can be used to define λ_0, λ_1, λ_2 or λ_3, according to the studied behaviour. Likewise, the three main sections of the water retention curve can be used to find these parameters.

The interpolation for the current tangent of the predicted curve requires the definition of at most two parameters in order to adjust how fast the initial behaviour approaches the reference behaviour. These parameters, $\overline{\beta}$ and $\overline{\overline{\beta}}$, are related to the curvatures of the smooth transitions. When $\overline{\beta}$ or $\overline{\overline{\beta}}$ are large, a bilinear model can be obtained. If these two parameters are set with large values at the same time, the equations convert into a trilinear model. Therefore, the calibration of the β parameters can be guided by the reference lines. Nonetheless, an automatic procedure for their determination is presented as well. This automatic procedure is based on some analytical equations that are solutions for the incremental model. With two references only, the model can be completely described by an analytical expression.

Several experimental results from mechanical and hydraulic tests were used in order to verify the equations proposed. These tests are related to three different geotechnical problems: isotropic compression of sands, water retention characteristics of geomaterials and volumetric behaviour of structured materials. In all cases, it has been demonstrated that the simulated results exhibit good agreements with the experimental data, proving the versatility and accuracy of the "reference curves" concept.

To sum up, the method proposed has the following advantages:

- Few parameters: two or three inclinations for some reference lines in addition to one or two smoothing (curvature) coefficients.

- Clear initial conditions, for example: initial void ratio or specific volume, initial degree of saturation or water content, initial effective mean stress or suction and initial reference points on some reference lines.
- Easy to find (automatically) parameters with the aid of analytical expressions, such as for the area below the predicted curves.
- Easy to be incorporated in a full non-linear (incremental) constitutive model. The $\mathrm{d}y/\mathrm{d}x = -\overline{\lambda}$ or $\mathrm{d}y/\mathrm{d}x = -\overline{\overline{\lambda}}$ tangent modulus are quite convenient when devising a stress–strain relationship, for example.
- Versatility: may be applied to smooth other bilinear or trilinear models, by means of the definition of reference lines or curves on the y–x plane defined with a pair of state variables.

Appendix A. Analytical solutions

The general form of a curve controlled by two reference lines is presented in Eq. (47). An analytical solution for this problem is given in Eq. (48), where the coefficients are function of an initial condition and the parameters. These coefficients are given by Eq. (51), where $(x_{\mathrm{ini}}, y_{\mathrm{ini}})$ represent a point on the $y(x)$ curve. The area below $y(x)$ curve can be calculated with the aid of Eq. (49), for a given x-range. The demonstration is as follows:

Given:

$$D = ax + by + c, \quad \lambda = A + (B - A)\mathrm{e}^{-\beta D} \quad \text{and} \quad \frac{\mathrm{d}y}{\mathrm{d}x} = -\lambda \tag{47}$$

Solution:

$$y = -Ax + \frac{1}{b\beta}\ln(c_3 + c_2\,\mathrm{e}^{c_1 x}) \tag{48}$$

$$S(x) = \int y(x)\mathrm{d}x = \frac{-Ax^2}{2} + \frac{1}{b\beta}L(x) \tag{49}$$

$$L(x) = x\ln(c_3 + c_2\,\mathrm{e}^{c_1 x}) - x\ln\left(1 + \frac{c_2}{c_3}\,\mathrm{e}^{c_1 x}\right)$$
$$- \frac{1}{c_1}\mathrm{li}_2\left(\frac{-c_2}{c_3}\,\mathrm{e}^{c_1 x}\right) \tag{50}$$

where li_2 is the dilog function and

$$c_1 = \beta(bA - a), \quad c_2 = \frac{A - B}{A - a/b}\,\mathrm{e}^{-c\beta} \quad \text{and}$$
$$c_3 = \mathrm{e}^{b\beta(y_{\mathrm{ini}} + Ax_{\mathrm{ini}})} - c_2\,\mathrm{e}^{c_1 x_{\mathrm{ini}}} \tag{51}$$

with the following restrictions:

$$b \neq 0 \quad \text{and} \quad A \neq a/b \tag{52}$$

Proof:
From Eq. (47),

$$\frac{\mathrm{d}y}{\mathrm{d}x} = -A - (B - A)\mathrm{e}^{-\beta(ax + by + c)}$$
$$= -A - (B - A)\mathrm{e}^{-a\beta x}\,\mathrm{e}^{-b\beta y}\,\mathrm{e}^{-c\beta} \tag{53}$$

resulting in the following ordinary differential equation:

$$\frac{\mathrm{d}y}{\mathrm{d}x} = -A - M\,\mathrm{e}^{-a\beta x}\,\mathrm{e}^{-b\beta y} \tag{54}$$

in which

$$M = (B - A)\mathrm{e}^{-c\beta} \tag{55}$$

This differential equation can be solved, after the definition of

$$u = \mathrm{e}^{b\beta y} \tag{56}$$

therefore,

$$\frac{\mathrm{d}u}{\mathrm{d}x} = b\beta u \frac{\mathrm{d}y}{\mathrm{d}x} = -b\beta Au - b\beta M\,\mathrm{e}^{-a\beta x} \tag{57}$$

which is a linear differential equation of the form

$$\frac{\mathrm{d}u}{\mathrm{d}x} = Nu + f(x) \tag{58}$$

where

$$N = -b\beta A \quad \text{and} \quad f(x) = -b\beta M\,\mathrm{e}^{-a\beta x} \tag{59}$$

The solution of this linear equation is given by (e.g. [12])

$$u = \mathrm{e}^{Nx}\left[c_3 + \int \mathrm{e}^{-Nx}f(x)\mathrm{d}x\right] \tag{60}$$

in which c_3 is an arbitrary constant, determined considering an initial point on the $y(x)$ curve. Substituting Eq. (59) into above solution,

$$u = \mathrm{e}^{-b\beta Ax}\left[c_3 - b\beta M \int \mathrm{e}^{\beta(bA - a)x}\mathrm{d}x\right] \tag{61}$$

thus, substituting Eq. (55) for M into above equation and simplifying,

$$u = \mathrm{e}^{-b\beta Ax}\left[c_3 + \frac{(A - B)\mathrm{e}^{-c\beta}}{A - a/b}\,\mathrm{e}^{\beta(bA - a)x}\right] \tag{62}$$

or, in a compact form,

$$u = \mathrm{e}^{-b\beta Ax}(c_3 + c_2\,\mathrm{e}^{c_1 x}) \tag{63}$$

where c_1 and c_2 are given in Eq. (51).

From Eq. (56),

$$y = \frac{\ln u}{b\beta} \tag{64}$$

After substitution of Eq. (63) into above equation, the solution given in Eq. (48) is obtained.

The constant c_3 can be found considering an initial point $(x_{\mathrm{ini}}, y_{\mathrm{ini}})$ on the $y(x)$ curve. In this way, from Eq. (63),

$$c_3 = u_{\mathrm{ini}}\,\mathrm{e}^{b\beta Ax_{\mathrm{ini}}} - c_2\,\mathrm{e}^{c_1 x_{\mathrm{ini}}} \tag{65}$$

in which, from Eq. (56),

$$u_{\mathrm{ini}} = \mathrm{e}^{b\beta y_{\mathrm{ini}}} \tag{66}$$

Thus, after substitution of the above expression into Eq. (65), the Eq. (51) for c_3 is obtained.

Appendix B. Computer codes

The following codes can be used with the free software/open source "R Project for Statistical Computing" [13]. Five functions are presented: (a) find.betas, which compute the area below data points and finds $\bar{\bar{\beta}}$ and $\bar{\beta}$ parameters; (b) L, correspondent to the auxiliary function $L(x)$ given in Eq. (50); (c) two.refs.model, which contains all code for the two references model; (d) three.refs.model1, for the three references – case 1 model; and (e) for the three references – case 2 model. The source code containing all these functions is also freely available at http://mechsys.nongnu.org.

The "find.betas" function, presented in Fig. 19, computes the area of two regions below a dataset, using smoothing via splines (Fig. 20). The first area (A1) is used to find $\bar{\bar{\beta}}$, with the aid of Eq. (7) based on the two references model. The second area (A2) is used to find $\bar{\beta}$, using Eqs. (14) or (32), depending on case 1 or 2, respectively. In this function, Xd and Yd are arrays of data points, for example, v (specific volume) and $\ln p$ (logarithm of effective mean stress). "ii" is the index of a inflection point in the Xd and Yd arrays. sp1 and sp2 are smoothing parameters for the spline function, in the range: $0 \leqslant sp \leqslant 1$; when $sp = 0$, the spline pass by all points; if $sp \sim 1$, the spline results in a smooth curve around all points.

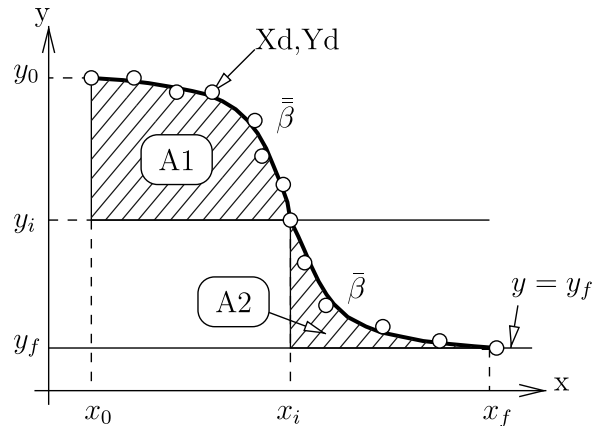Figs. 21–24 present the codes for the functions $L(x)$, two.refs.model, three.refs.model1, and three.refs.model2, respectively. Incremental and analytical equations are provided. For three.refs.model 1 or 2, the analytical equations are given for the reference curves $y_1(x)$ or $y_3(x)$, respectively. L0, L1, L2 and L3 stand for λ_0, λ_1, λ_2 and λ_3. Bb and Bbb indicate $\bar{\beta}$ and $\bar{\bar{\beta}}$. x0, y0, xR10, yR20 and xR30 stand for x_0, y_0, x_{R1}^0, y_{R2}^0 and x_{R3}^0. These last five variables correspond to the initial values necessary to set up a reference model. The functions return the $y(x)$ functions, the auxiliary functions $S(x)$ to compute the area, and the tangent modulus, as summarized in Table 1.

Fig. 20. Areas computed with function "find.betas".

```
find.betas <- function(L0,L1,Xd,Yd,ii,sp1,sp2,case2=FALSE,L2=NULL,L3=NULL) {
    # compute area from data
    s1 <- smooth.spline(Xd[1:ii],Yd[1:ii],spar=sp1)
    s2 <- smooth.spline(Xd[ii:n],Yd[ii:n],spar=sp2)
    f1 <- function(x) { predict(s1,x)$y-yi }
    f2 <- function(x) { predict(s2,x)$y-yn }
    A1 <- area(f1,x0,xi)
    A2 <- area(f2,xi,xn)
    # find Bbb from A1
    g1 <- function(Bbb) {
        if (case2) {
            r <- two.refs.model(L0,L1,Bbb, x0,y0,xR10)
            A <- (r$S(xi)-r$S(x0))-(yi*(xi-x0)) }
        else {
            r <- two.refs.model(L0,L3,Bbb, x0,y0,xR30)
            A <- (r$S(xi)-r$S(x0))-(yi*(xi-x0)) }
        return ((A-A1)^2)
    }
    o1  <- optimize(g1, c(0.1,20), tol=0.001)
    Bbb <- o1$minimum
    # find Bb from A2
    g2 <- function(Bb) {
        if (case2) {
            r <- three.refs.model1(L0,L1,L2,Bb,Bbb, x0,y0,xR10,yR20)
            A <- (r$S1(xn)-r$S1(xi))-(yn*(xn-xi))
        else {
            r <- three.refs.model2(L0,L1,L3,Bb,Bbb, x0,y0,xR10,xR30)
            A <- (r$S3(xn)-r$S3(xi))-(yn*(xn-xi))
        }
        return ((A-A2)^2)
    }
    o2 <- optimize(g2, c(0.1,20), tol=0.001)
    Bb <- o2$minimum
}
```

Fig. 19. Code for "find.betas" function.

```
L <- function(c1,c2,c3,x) {
   return (   x*log(c3+c2*exp(c1*x))
            - x*log(1 +c2*exp(c1*x)/c3)
            - dilog(  -c2*exp(c1*x)/c3)/c1)
}
```

Fig. 21. Code for *L(x)* auxiliary function.

```
two.refs.model <- function(L0,L1,Bb, x0,y0,xR10) {
   # incremental
   xR1   <- function(y)    { xR10+(y0-y)/L1                }
   Db    <- function(x,y) { xR1(y)-x                       }
   Lb    <- function(x,y) { L0+(L1-L0)*exp(-Bb*Db(x,y))    }
   dSdy  <- function(x,y) {  -1/Lb(x,y)                    }
   dEdx  <- function(x,y) {    -Lb(x,y)                    }
   # analytical
   c1    <- Bb*(1-L0/L1)
   c2    <- exp(-Bb*(xR10+y0/L1))
   c3    <- exp(-Bb*(y0+L0*x0)/L1)-c2*exp(c1*x0)
   y     <- function(x) { -L0*x-L1*log(c3+c2*exp(c1*x))/Bb }
   S     <- function(x) { -0.5*L0*x^2-L1*L(c1,c2,c3,x)/Bb  }
   return (list(dSdy=dSdy, dEdx=dEdx, y=y, S=S))
}
```

Fig. 22. Code for the model with two references.

```
three.refs.model1 <- function(L0,L1,L2,Bb,Bbb, x0,y0,xR10,yR20) {
   # arrays:
   #     S = {x,xR1}
   #     E = {y,xR1}
   # incremental
   yR2   <- function(x)       { yR20-L2*(x-x0)                          }
   Db    <- function(x,y)     { y-yR2(x)                                }
   Dbb   <- function(x,y,xR1) { xR1-x                                   }
   Lb    <- function(x,y)       { L1+(L2-L1)*exp(-Bb*Db(x,y))           }
   Lbb   <- function(x,y,xR1) { L0+(Lb(x,y)-L0)*exp(-Bbb*Dbb(x,y,xR1))  }
   dSdy  <- function(y,S)     { -1 / c( Lbb(S[1],y,S[2]), Lb(S[1],y) )  }
   dEdx  <- function(x,E)     { Lbb(x,E[1],E[2]) / c( -1, Lb(x,E[1]) )  }
   # analytical expressions
   c1 <- Bb*(L1-L2)
   c2 <- exp(Bb*(yR20+L2*x0))
   c3 <- exp(Bb*(y0+L1*xR10))-c2*exp(c1*xR10)
   y1 <- function(x) { -L1*x+log(c3+c2*exp(c1*x))/Bb }
   S1 <- function(x) { -0.5*L1*x^2+L(c1,c2,c3,x)/Bb  }
   return (list(dSdy=dSdy, dEdx=dEdx, y1=y1, S1=S1))
}
```

Fig. 23. Code for the model with three references – case 1.

```
three.refs.model2 <- function(L0,L1,L3,Bb,Bbb, x0,y0,xR10,xR30) {
   # arrays:
   #     S = {x,xR3}
   #     E = {y,xR3}
   # incremental
   xR1   <- function(y)       { xR10+(y0-y)/L1                             }
   Db    <- function(x,y,xR3) { xR3-xR1(y)                                 }
   Dbb   <- function(x,y,xR3) { xR3-x                                      }
   Lb    <- function(x,y,xR3) { L3+(L1-L3)*exp(-Bb*Db(x,y,xR3))            }
   Lbb   <- function(x,y,xR3) { L0+(Lb(x,y,xR3)-L0)*exp(-Bbb*Dbb(x,y,xR3)) }
   dSdy  <- function(y,S)     { -1 / c( Lbb(S[1],y,S[2]), Lb(S[1],y,S[2]) ) }
   dEdx  <- function(x,E)     { Lbb(x,E[1],E[2]) / c( -1, Lb(x,E[1],E[2]) ) }
   # analytical expressions
   c1 <- Bb*(L3/L1-1)
   c2 <- exp(Bb*(xR10+y0/L1))
   c3 <- exp(Bb*(y0+L3*xR30)/L1)-c2*exp(c1*xR30)
   y3 <- function (x) { -L3*x+L1*log(c3+c2*exp(c1*x))/Bb }
   S3 <- function (x) { -0.5*L3*x^2+L1*L(c1,c2,c3,x)/Bb  }
   return (list(dSdy=dSdy, dEdx=dEdx, y3=y3, S3=S3))
}
```

Fig. 24. Code for the mode with three references – case 2.

References

[1] Clementino RV. Discussion of "An oedometer test study on the preconsolidation stress of glaciomarine clays". Can Geotech J 2005;42:972–4.

[2] Cunningham MR, Ridley AM, Dineen K, Burland JB. The mechanical behaviour of a reconstituted unsaturated silty clay. Géotechnique 2003;53(2):183–94.

[3] Fredlund DG, Rahardjo H. Soil mechanics for unsaturated soils. New York, USA: John Wiley and Sons; 1993. p. 517.

[4] Lade PV, Bopp PA. Relative density effects on drained sand behavior at high pressures. Soil Found 2005;45(1):1–14.

[5] Lagioia R, Nova R. An experimental and theoretical study of the behaviour of a calcarenite in triaxial compression. Géotechnique 1995;45(4):633–48.

[6] Lee KL, Seed HB. Drained characteristics of sands. ASCE J Soil Mech Found Div 1967;93:117–41.

[7] Lins Y, Zou Y, Schanz T. Physical modeling of SWCC for granular materials: theoretical and numerical unsaturated soil mechanics. Germany: Weimar; 2007.

[8] Liu MD, Carter JP. A structured Cam clay model. Research report no. R814. The University of Sydney, Department of Civil Engineering, Sydney, Australia; 2002. p. 1–68.

[9] Nahlawi H, Bouazza A, Kodikara J. Characterisation of geotextiles water retention using a modified capillary pressure cell. Geotext Geomembr 2007;25(3):186–93.

[10] Nakano M, Nakai K, Noda T, Asaoka A. Simulation of shear and one-dimensional compression behavior of naturally deposited clays by super/subloading yield surface Cam-clay model. Soil Found 2005;45:141–51.

[11] Pestana JM, Whittle AJ. Compression model for cohesionless soils. Géotechnique 1995;45(4):611–31.

[12] Polyanin AD, Zaitsev VF. Handbook of exact solutions for ordinary differential equations. Boca Raton: Chapman and Hall/CRC press; 2003. p. 816.

[13] R Development Core Team. R: a language and environment for statistical computing, R foundation for statistical computing, Vienna, Austria; 2006 [ISBN: 3-900051-07-0]. <http://www.r-project.org>.

[14] Schofield A, Wroth P. Critical state soil mechanics. McGraw Hill; 1968. p. 218.

[15] Sheng D, Fredlund DG, Gens A. A new modelling approach for unsaturated soils using independent stress variables. Research report. Australia: The University of Newcastle; 2006 [ISBN: 1920701761].

[16] Sheng D, Sloan SW, Gens A, Smith DW. Finite element formulation and algorithms for unsaturated soils. Part I: Theory. Int J Numer Anal Method Geomech 2003;27:745–65.

[17] Sheng D, Yao YP. A volumetric stress–strain model for sands experiencing particle crushing 2007:1–12.

[18] Yao YP, Sun DA, Luo T. A critical state model for sands dependent on stress and density. Int J Numer Anal Method Geomech 2004;28:323–37.